HiSST: 3rd International Conference on
High-Speed Vehicle Science Technology
14 -19 April 2024, Busan, Korea

Design of pulsed magnetic circuit with Pulse Forming Network for experimental study of Magnetohydrodynamic aerobraking

T. Muramatsu [1], Y. Kurosaka [1], K. Shimamura [1], A. Kakami [1], H. Katsurayama [2]
Tokyo Metropolitan Univ.[1], Tottori Univ.[2]

Abstract

In this paper, a magnetic circuit is designed for the study of MHD aerobraking using a pulsed magnetic field in a hypersonic wind tunnel (Expansion tube). The magnetic circuit is composed of a magnetic field generating coil, a Pulse Forming Network (PFN) as a power source, and a drive circuit centered on IGBT. A magnetic field generating coil with a diameter of 12 mm was fabricated, confirming a magnetic field density of 1.3 T on the specimen surface. Subsequent wind tunnel tests, utilizing the fabricated magnetic circuit, resulted in the acquisition of self-luminous images. A comparison of these images revealed a difference of approximately 15% in the self-luminous region. These results suggest that the application of pulse magnetic fields to the test airflow confirmed changes in the shock wave layer.

Keywords : *MHD Aerobraking, Pulse Forming Network, Shock layer*

Nomenclature

v – Airflow velocity
B – Magnetic Flux Density
J_θ – Circumferential current
C – Capacitance
L – Inductance
L_s – Characteristic length (specimen diameter)
ρ – Air flow density
σ – Electrical conductivity
d_i – coil diameter
d_c – cable diameter

1. Introduction

During atmospheric re-entry, the spacecraft's flight speed is extremely high and a shock wave is formed in front of the body. As a result, the surface of the spaceplane is exposed to high temperatures due to aerodynamic heating caused by adiabatic compression of the shock wave. Passive thermal protection systems such as ablators and heat-resistant tiles have been used against aerodynamic heating. However, such systems have problems such as difficulty in reuse and efficiency of thermal protection. These problems call for efficient active thermal protection systems that are lightweight, reusable, and directly reduce heat inflow. Accordingly, various universities and research institutes are studying active thermal protection systems. Magnetohydrodynamic (MHD) aerobraking: Fig 1 is one such candidate [1].

Many experimental studies on MHD aerobraking have been conducted in arc wind tunnel and Expansion tube [2-3]. As a result, an increase in the shock layer and a change in the heat flux have been observed when a magnetic field is applied. However, all the aforementioned experiments were conducted using neodymium magnets as the magnetic field source, making it difficult to measure clear differences due to the limitations of magnetic flux density. Therefore, a magnetic field source with a large magnetic flux density is required to clearly observe distinctions.

In response to the above problem, experiments are currently being conducted utilizing pulse magnetic fields and superconductors capable of generating stronger magnetic fields. In experiments utilizing superconducting coils, resulting in the generation of approximately 4.5T magnetic fields, a clear variation in shock stand-off distance was observed [4]. However, due to structural influences such as cooling mechanisms, models employing superconducting coils tend to be enlarged. Consequently, there

are fewer instances of experiments compared to those using permanent magnets, and no examples of synchronization with Expansion tube have been observed.

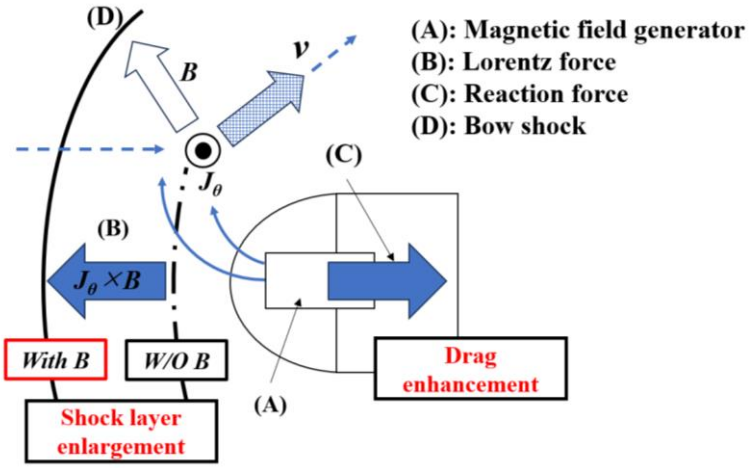

Fig 1. MHD Aerobraking

In consideration of the foregoing, experiments were conducted utilizing a pulsed magnetic field capable of generating a magnetic field greater than that of a permanent magnet with minimal cooling, despite the magnetic field maintenance time being as short as 1ms. In this study, to mitigate the rapid decay of the magnetic field associated with the use of an ordinary capacitor as the power source for the magnetic field generator circuit, an LC ladder circuit known as a Pulse Forming Network was employed as the primary power source. The magnetic circuit was synchronized to the test time of the Expansion tube, and changes in the shock layer were observed using a high-speed camera.

2. Experimental procedure

2.1. Pulse Forming Network

The Pulse Forming Network (PFN) is a power source constructed using capacitors and coils, generating relatively long pulse currents of several nanoseconds or more. Fig 2 illustrates the theoretical voltage waveform when a single-stage capacitor is used and presents the measured current waveform of the PFN. Each axis represents time [μs] on the horizontal axis and output voltage [V] or output current [A] on the vertical axis.

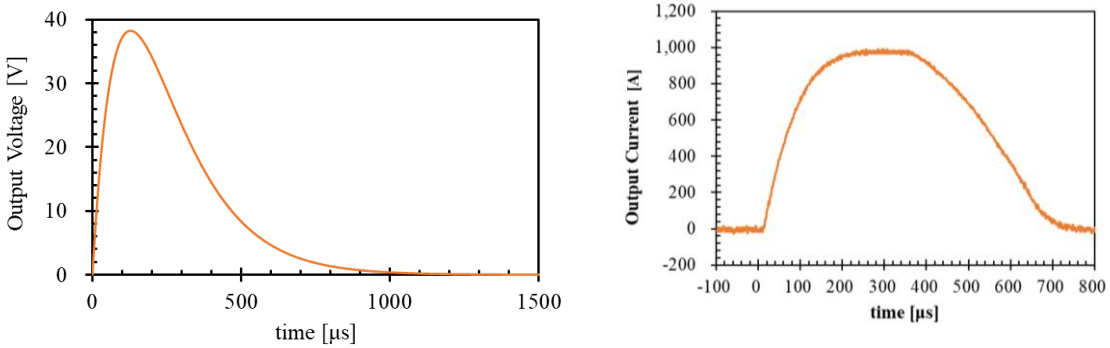

(A) (B)

Fig 2. Comparison of output waveforms of single-stage capacitor and PFN

As evident from the above Figure, with discharge from a single-stage capacitor, the voltage increases to its maximum value, then quickly decreases without achieving a constant voltage. In contrast, the output current of the PFN reaches its maximum value, followed by a nearly constant current region. It is possible to generate a quasi-steady magnetic field using this constant region. In this study, the PFN and the coil serving as the load were impedance-matched to accommodate the sub-millisecond testing duration of the expansion tube. They were constructed to have a pulse width of approximately 1 ms. Furthermore, the charging voltage was set at 420V, considering it as the value capable of generating 1

kA in the magnetic field generation coil. Additionally, a drive circuit including IGBTs capable of high-speed response and withstanding high currents was fabricated to serve as the switch to initiate the output from the PFN. The discharge of the magnetic circuit initiates within 150 μs from the trigger signal. The image of the PFN is shown in Fig 3, and the configuration parameters of the PFN are presented in Table 1.

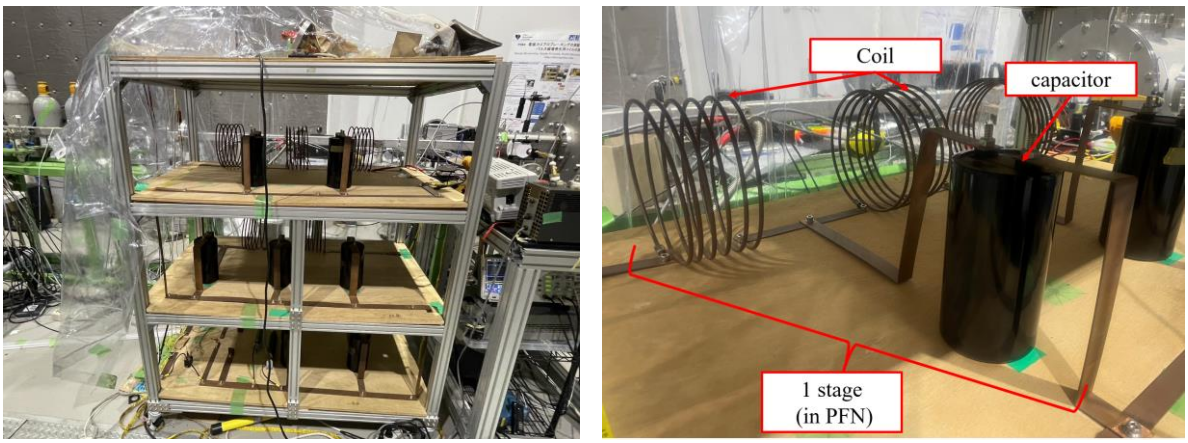

(A) (B)

Fig 3. Pulse Forming Network

(A): exterior view, (B): detailed view

Table 1. PFN Specifications

Capacitance: C [μF]	730 ± 10%
Permissible voltage [V]	800
Inductance: L [μH]	7.0
Number of steps	7
Discharge time [ms]	1±10%
Maximum charge voltage [V]	420
Characteristic Impedance [mΩ]	100

2.2. Magnetic field generating coil

The magnetic field generating coil was designed using FEMM (Finite Element Method Magnetics), a static magnetic field analysis software based on the finite element method. The coil bobbin was fabricated using a 3D printer (filament from Formlabs' High Temp Resin). Fig 4 presents the coil within the specimen, along with the appearance during the insertion of the test section. The structure is designed to integrate the bobbin and the blunt-nosed test specimen. The aim is to position the region of high magnetic flux density at the center of the bobbin closer to the airflow. The d_i and the test specimen diameter is 12mm and 20mm, respectively. The coil winding was made of polyurethane copper wire. The d_c was 0.5 mm, and the wire was wound 49 times on a bobbin. The magnetic flux density at the surface of the specimen was determined to be about 1.3 T from measurements using a pickup coil. In Table 2, a comparison is being made between the produced coils and the results of the FEMM analysis used in the design.

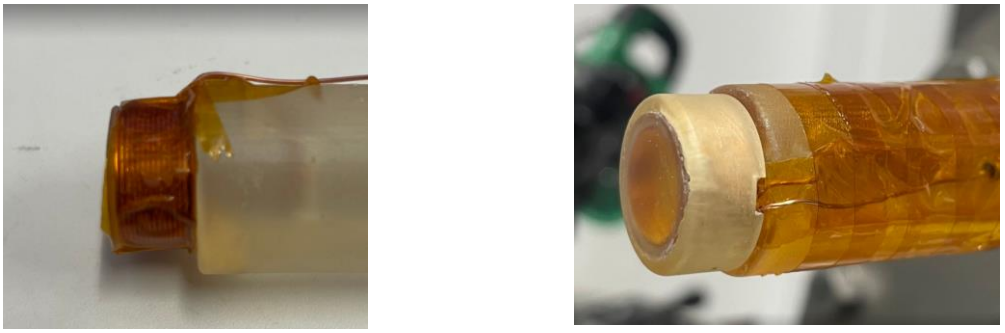

(A) (B)

Fig 4. Manufactured a magnetic field generating coil
(A): Internal coil, (B): Overall view

Table 2. Comparison between the produced coils and FEMM analysis results

	experimental	FEMM
coil resistance [Ω]	0.199	0.186
impedance [Ω]	0.244	0.253
inductance [μH]	22.6	27.4

2.3. Operation of Expansion tube and Synchronization with Magnetic Circuit

As illustrated in Fig 5, the expansion tube is comprised of the Compression tube, Shock tube, Acceleration tube, test section, and dump tank, arranged from left to right on the page. Helium was supplied to the Compression tube, while air was supplied to the Shock tube and Expansion tube. Between the compression tube and the shock tube, a first diaphragm with a central cross groove is installed, and between the Shock tube and the Expansion tube, a 12μm-thick Mylar diaphragm is placed as the second diaphragm. The operational conditions are presented in Table 3.

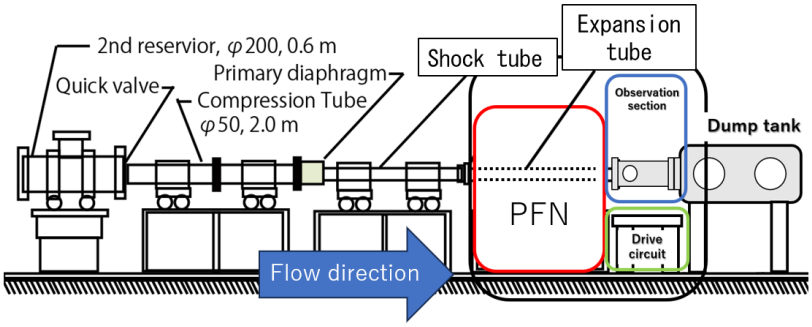

Fig 5. Expansion tube

Table 3. Expansion tube operating condition

Secondary reservoir	1 MPa
Driver gas	He
Shock / Acceration tube gas	Air / Air
Driver gas pressure	40 kPa
Shock tube fill pressure	60 Pa
Acceration tube fill pressure	10 Pa
Free piston	Al, 281 g
Primary Diaphgram	spcc, 1.6 mm
Secondary Diaphgram	mylar, 12 μm

Furthermore, the test time of the Expansion tube was identified through dynamic pressure measurements using a pitot tube. The test time was defined to commence 14μs after the arrival of the shock wave and conclude at 50μs when the pressure fluctuations became significant. The airflow conditions are presented in Table 4.

Table 4. Test flow conditions

Acceleration tube shock speed [km/s]	7.54
Free stream velocity [km/s]	7.00
Pitot pressure[kPa]	173
air flow density [g/m^3]	3.10
Shock layer electrical conductivity[Ω^{-1} ・ m^{-1}]	2860
Test time[μs]	40

The synchronization between the magnetic circuit and the expansion tube is accomplished using the rise signal indicating the arrival of the Shock wave from the static pressure sensor located 600 mm from the first diaphragm. The rise signal is input into the Delay Generator (STANFORD RESEARCH SYSTEMS, INC., DG535), where an appropriate delay time is applied before the TTL signal is emitted to the drive circuit of the magnetic circuit. In addition, the trigger signal for the high-speed camera used for shock layer measurement was also emitted from the Delay Generator.

2.4. Measurement device

The detachment distance of the shock wave layer was measured from the self-luminous images captured by the high-speed camera (HX-3: nac Image Technology Inc.). Additionally, self-luminous from the surface of the test specimen at a position 1mm away was collected and input to the photodetector (DET10A2: Thorlabs) to detect the arrival timing of the shock wave. The test flow was directed from left to right across the page. Fig 6 depicts the arrangement of the high-speed camera and condenser lens.

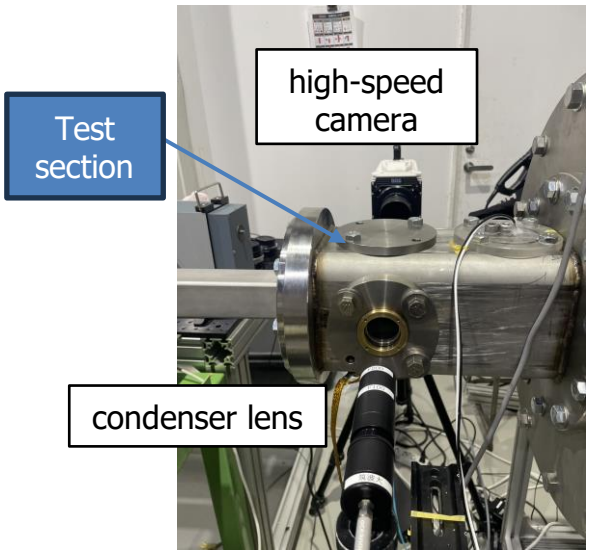

Fig 6. Arrangement of observation systems

3. Experimental results

3.1. Synchronization of Expansion tube and Magnetic Circuit

The synchronization results between the magnetic circuit and the expansion tube are depicted in Fig 7. It is observed from the graph that around 250μs, there is a rise signal from the photodetector indicating the arrival of the shock wave. At this point, the maximum current output from the PFN is achieved. Since the increase in magnetic field follows the output current, it is presumed that the application of the magnetic field was synchronized with the test time of the Expansion tube.

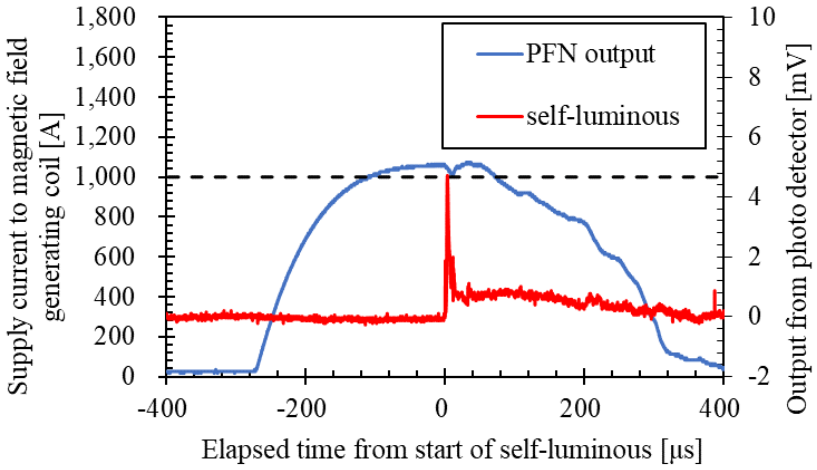

Fig 7. Synchronization results between Expansion wave tube and magnetic circuit

3.2. Measurement results of self-luminous image

The self-luminous images captured by the high-speed camera are presented in Fig 8 (A). In the following figures, images from tests #208 and #219 are compared, starting at 14μs and 13μs after the initiation of the test time, respectively. The upper half of the image is shown before the magnetic field was applied, and the lower half is shown after the field was applied.

It is observed that the self-luminous light region inside the shock layer is slightly increased by the application of the magnetic field. The expansion of the self-luminous region is thought to be attributable to the trapping of electrons by the magnetic field generated radially from the specimen surface. Furthermore, it is considered that the positions of the luminescent region's end face and the shock stand-off distance coincide at the airflow velocities examined in this research. It is suggested that the shock stand-off distance is increased along with the expansion of the self-luminous region.

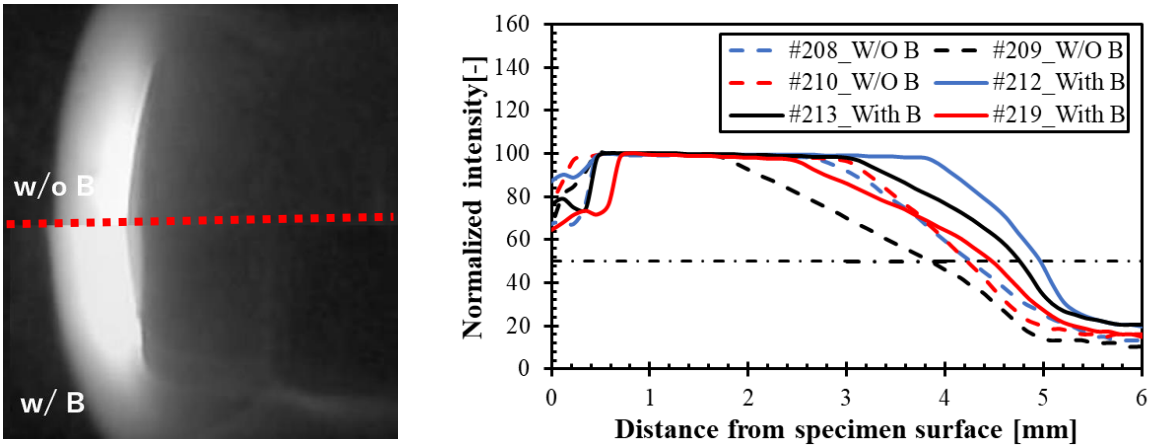

(A) (B)

Fig 8. (A) : Comparison of self-luminous images before and after application of magnetic field
(B) : Comparison of self-luminous intensity (34μs from start of test time)

From the above results, it was judged that a magnetic field could be applied to the test flow, and a quantitative comparison was conducted. The method involved using Image J to derive the luminance intensity along the stagnation point line (above the red dotted line). The results are shown in Fig 8 (B) , with the distance from the stagnation position [mm] on the horizontal axis and the normalized self-luminescence intensity on the vertical axis. The comparison was made around 34μs after the start of the test time. Normalization was performed by dividing by the maximum intensity of each shot. As can be seen above figure, the self-luminescence area after the application of the magnetic field (solid line) increases compared to the area before the application of the magnetic field (dotted line), indicating that the self-luminescence area is quantitatively expanded.

Additionally, since this study was unable to accurately capture the shock stand-off distance, the positions marked by the dashed lines at 50% in the Fig 8(B) were used as a reference for the shock stand-off distance and compared during the test period. As a result, an increase in the stand-off distance from 4.14mm before the application of the magnetic field to 4.78mm after its application was observed, representing an approximate 15% increase in the stand-off distance.

3.3. Relationship between Q parameter and Shock stand-off distance

The parameter Q can be calculated as shown in Eq. 1, where the numerator corresponds to the Lorentz forces and the denominator to the inertial forces of the airflow. Hence, a condition where Q exceeds 1 indicates that electromagnetic forces surpass the airflow's inertial forces, facilitating a pushing out effect of the shock layer under certain conditions of airflow and mechanisms of magnetic field generation. In the equation, the symbols are defined as follows: σ for electrical conductivity, B for magnetic flux density, Ls for characteristic length, ρ for airflow density, and v for airflow velocity.

$$Q = \frac{\sigma B^2 L_s}{\rho v} \tag{1}$$

In the experiments conducted, the Q parameter for each shot was calculated using the conditions of the test flow, yielding an average value of 4.1. This indicates that under the magnetic field generation mechanism and airflow conditions employed in this study, changes in the shock wave layer are possible. Furthermore, Lykoudis has derived a relationship for the nondimensional stand-off distance of a spherical model with respect to the Q parameter [5]. In Fig 9, a comparison between the results obtained in this study and theoretical values is presented, with the Q parameter on the horizontal axis and the dimensionless stand-off distance on the vertical axis.

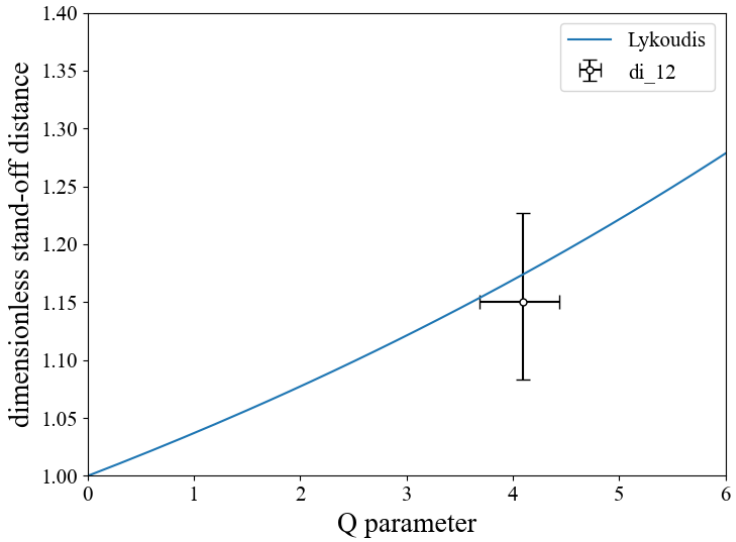

Fig 9. Relationship between Q parameter and dimensionless stand-off distance

From the results above, it is evident that the observed expansion ratio from the self-luminous region in this study is close to the theoretical values for the Q parameter. This suggests that the findings of this research are valid. However, since the stand-off distance of the shock wave is defined based on self-luminous images in this study, it is necessary to employ other verification methods, including schlieren technique, in future investigations.

Conclusion

This study successfully constructed a magnetic circuit for generating pulse magnetic fields with a Pulse Forming Network, achieving a magnetic field of approximately 1.3 T. Furthermore, it was confirmed that the magnetic circuit is capable of synchronizing with the 40μs test time of the Expansion tube. Upon comparing images before and after the application of a magnetic field, an expansion of the luminous region within the shock layer was observed. Specifically, the luminous region saw a 15% increase in size compared to the state before magnetic field application, suggesting that the shock stand-off distance was also altered as a result. Future directions for this research include diversifying verification methods through thermal flux measurements, varying the types of test gases used, and enhancing the magnetic circuit to increase magnetic flux density.

References

1. H. Otsu and T. Abe: Flow field control around re-entry flight vehicles by electromagnetic force and its application (in Japanese), Journal of the Japan Society for Aeronautical and Space Sciences 59-692: 268-272 (2011)
2. H. Katsurayama, D. Konigorski, and T Abe: Numerical Simulation of Electromagnetic Flow Control in a One-Kilowatt Class Argon Arcjet Windtunnel, 39th Plasmadynamics and Lasers Conference, June 23-26, Seattle, Washington, 2008-4016.
3. D. Gildfind, D. Smith, S. Lewis, H. Wei, C. James, and T. McIntyre: Expansion Tube Test Flow Design for MHD Experimentation, 12th International Workshop on Shock Tube Technology, April 13, 2018.
4. J. M. Schramm, and K. Hannemann: Study of MHD Effects in the High-Enthalpy Shock Tunnel Göttingen (HEG) Using a 30 T-Pulsed Magnet System, ISSW31, July 9-14, Nagoya, Japan, 2017, 617-623.
5. Paul S. Lykoudis: The Newtonian Approximation in Magnetic Hypersonic Stagnation-Point Flow, Journal of the Aerospace Sciences(1961), https://doi.org/10.2514/8.9073